A modeling-based assessment of the imprint of storms on wind waves in the Western Mediterranean Sea

T. Toomey*[1] , J.M. Sayol[2] , M. Marcos[3,4] , G. Jordà[3,4] , J. Campins[5]

[1]ENSTA-Bretagne, Department STIC-HOP, Brest, France
[2]Delft University of Technology, Department of Hydraulic Engineering, Delft, The Netherlands
[3]Department of Physics, University of the Balearic Islands, Palma, Spain
[4]IMEDEA (UIB-CSIC), Esporles, Spain
[5]Agencia Estatal de Meteorología (AEMET), Palma de Mallorca, Spain

Keywords:

Western Mediterranean Sea, atmospheric cyclones, wind-wave climate, wind climate

---

*Corresponding author: T. Toomey, tim.toomey@ensta-bretagne.org
tim.otuma@gmail.com

Abstract

This study analyzes the distribution of ocean wind waves in response to extra-tropical cyclones over the Western Mediterranean Sea. To this end we use an ERA40-based database of atmospheric cyclones and a 3-hourly wind wave hindcast with high horizontal resolution ($\frac{1}{6}$°) based on an ERA40 downscaled forcing for the region of study. The imprint of winds on surface waves is evaluated through composites of modeled significant wave height, surface wind and wave peak period collocated under the storms. Results highlight an asymmetric pattern that depends on the translational speed and size of the cyclonic perturbations. Uncertainties of the composites are at most 10% at 95% confidence interval, with an average maximum perturbation of significant wave height near 2 m for those cyclones moving faster than 10 m/s.

1 Introduction

In recent years a great effort has been dedicated to better understand the formation and propagation of ocean surface waves under the presence of atmospheric cyclones. Due to the major threat that they represent, there have been historically many works focused on tropical cyclones (TCs) (see e.g. Cline, 1920; Tannehill, 1936; Wright *et al.*, 2001; Moon *et al.*, 2003, 2004; Fan *et al.*, 2009; Doyle *et al.*, 2012; Holthuijsen *et al.*, 2012; Stephens and Ramsay, 2014; Timmermans *et al.*, 2017). Conversely, less attention has been paid to extra-tropical cyclones, being most of the works focused on particular events occurring in North and South Atlantic Ocean (see e.g. Cardone *et al.*, 1996; Innocentini and Neto, 1996; da Rocha *et al.*, 2004; Guimarães *et al.*, 2014). A good example of that is the Mediterranean Sea basin, with one of the highest rates of cyclogenesis in the world (Jansà, 1997; Sartini *et al.*, 2015). There, low-pressure perturbations develop quickly due to the interaction of the air with the mountains surrounding the basin. Compared to TCs, these extra-tropical lows are weaker, smaller and shorter-living. Even so, their intense wind and torrential rain are enough to give rise to periodically harmful events with a huge amount of material loss and, occasionally, of human lives. Coastal floods by storm surges and strong beach erosion and damage on marine infrastructures by waves are recurrent during these events (see e.g. De Zolt *et al.*, 2006; Harley *et al.*, 2017).

This study focuses on the Western Mediterranean, where the formation of cyclones or the intensification of other low-pressure disturbances traveling from the Atlantic Ocean or North of Africa places that region as one of the most active of the Northern Hemisphere (Jansà, 1997; Campins et al., 2011). The Mediterranean region favors a wide range of mechanisms as formation or deepening of mid-latitude perturbations by the orography and their fueling by low-level baroclinicity and/or low-level moisture sources (Trigo *et al.*, 2002). Origin, properties (e.g. size, structure and lifetime) and paths of cyclones in the Mediterranean Sea have been the subject of previous research (a complete review is presented in Lionello *et al.*, 2006). As a result, there are available databases of storms including their trajectory, center position and size (see e.g. Campins *et al.*, 2011; Dacre *et al.*, 2012).

Recently Besio *et al.* (2017) have discussed the spatial distribution of wave storms sequences in the Mediterranean Sea from a coastal hazard perspective using a wave hindcast. Alternatively, here we take advantage of the existence of simultaneous cyclone tracks and a high resolution wave hindcast to analyze the spatial distribution of ocean surface waves under atmospheric cyclones in the Western Mediterranean Sea. More in detail, we are interested in answering the following three questions: do these weaker extra-tropical cyclones leave a clear signature on ocean surface waves? How this pattern changes with cyclone properties (different size, translational velocity or direction of propagation)? How do their imprints compare to those of TCs? To respond to these questions we have performed composites of significant wave height, wave peak period and surface wind field collocated under atmospheric cyclones.

The article is organized as follows: Section 2 introduces the database of cyclones and the wave reanalysis; Section 3 describes the methodology followed to make the composites; Section 4 presents the composites of wave and wind fields for cyclones grouped by size and translational speed; finally, Section 5 discusses the results and outlines the main conclusions.

2 Data

A cyclone climatology for the Mediterranean Sea spanning the period 1958-2001 and based on ERA40 re-analysis mean sea level pressure data set has been used (Campins *et al.*, 2011). It consists of 6-hourly positions, timing and radii (assuming a circle) of a total of 81762 observations corresponding to 34612 different cyclones. The spatial resolution is 1.125° in both latitude and longitude (≈ 125 km), derived using the tracking algorithm firstly presented by Picornell *et al.* (2001) and further developed in (Campins *et al.*, 2011). The robustness of this method has been confirmed by Lionello *et al.* (2016) through an inter-comparison of 14-cyclone detection and tracking methods using the ERA Interim reanalysis. Despite the different spatial resolution of ERA40 and ERA-Interim wind fields it is expected that the size and center of cyclones (and then the cyclonic wind fields) will be similar for the big moving cyclones here studied, with an average radii of 500 km.

To investigate the wave climate in the basin, a wind wave reanalysis over the Western Mediterranean Sea has been used. It has been generated using the WAM model (The Wamdi Group, 1988), in a grid of $\frac{1}{6}$ ° of spatial resolution fed with 10-m wind fields obtained from ARPERA, a dynamical downscaling of ERA40 with a spatial resolution over the Mediterranean

Sea of 40-50 km (Jordà *et al.*, 2012; Martínez-Asensio *et al.*, 2013). The ARPERA hindcast simulation covers the period 1958–2001 and has been run using a global stretched-grid version of the ARPEGE-Climate model (Déqué and Piedelievre, 1995; Déqué, 2007). The ARPERA dataset is temporally consistent over the entire period and provides realistic interannual variability (nudging towards ERA40). Moreover, its resolution of 50 km has been demonstrated to be enough to significantly improve the representation of the extremes over the sea (Jordà et al 2012). Output fields consist of 3-hourly values of the wave parameters, namely significant wave height (Hs), calibrated by Martínez-Asensio *et al.* (2013) on the basis of in-situ buoy observations, wave direction and wave peak period (T_p). Wind-sea ($H_s^{wind\text{-}sea}$) and swell (H_s^{swell}) components of significant wave height are also provided separately. The corresponding monthly mean field of each wave parameter at each grid point has been removed (except for T_p), as we focus on the imprint of winds generated by cyclones on surface waves. Therefore, all the results presented hereinafter correspond to wave anomalies, unless otherwise stated.

3 Methods

To explore the impact of cyclones on the wave climate, we have selected those events whose center and at least 50% of their surface are located over the sea. This threshold has been chosen as a trade-off to ensure that the impact of cyclones occurs mostly over the sea surface and that the number of cyclones to be analyzed is large enough. Furthermore, we have kept the cyclones with a non-zero translational speed (TS). The TS has been calculated as the ratio between the distance and time at two consecutive time steps. This reduces the initial data set to 5178 observations corresponding to 2537 different cyclones (see their spatial distribution in Figure S1).

As expected, most of the cyclones are located around the Gulf of Genoa (Figure S1), known to be an active region in terms of cyclogenesis in the Western Mediterranean (Jansà, 1997; Trigo *et al.*, 1999; Maheras *et al.*, 2001; Nissen *et al.*, 2010; Campins *et al.*, 2011). The same pattern arises when intensity of cyclones (further defined in section 4.2) is mapped. Among all the observations considered, 35.59% of cyclones occur during the winter season. In addition, when only the strongest 10% events are concerned, almost half of them occur in winter (45.71%) in agreement with earlier studies (Trigo *et al.*, 1999; Maheras *et al.*, 2001; Besio *et al.*, 2017).

For each of the selected cyclones and at every time step, collocated wave fields are extracted over the sea area covered by the cyclone. We have kept all time steps for each cyclone, instead of that of maximum intensity, because in this region the intensity does not show large variations during the cyclone life time and because a reduced number of cases would diminish the statistical significance of the analyses. Therefore, unlike with large scale intense extra-tropical storms (Rudeva and Gulev, 2007), we have considered that the imprint on waves is equally important during all cyclone stages. The wave fields associated to each individual cyclone have undergone a two-step transformation. Firstly, the wave fields are rotated so that the corresponding cyclone direction is set upwards. Secondly, the wave fields are normalized according to each cyclone radius. Normalized and rotated wave fields are then linearly interpolated onto a regular grid of 301 × 301 points, so the resulting fields are comparable to each other, irrespective of the size of the cyclone. Composites are built by averaging normalized and rotated wave fields. Their uncertainties are calculated as the 95% confidence interval over the mean value (ME: Margin error), assuming a t-Student distribution. In addition to the wave parameters provided by the numerical simulation, the impact of the cyclones on the wave age (WA) has also been explored. Finally, the relationship between the maximum Hs and maximum wind speed has been quantified using an empirical polynomial formula.

Despite the cyclone tracks database and the wave reanalysis have been generated from slightly different wind fields it is expected that the cyclonic surface wind field matches reasonably well with the size and position of the cyclone. Figure 1 presents the tracking of one cyclone with the surface wind field superimposed for successive time steps. Additionally, the composite of the wind field for all cyclones shown in Figure S2 confirms a good general agreement, except for a little displacement of the center, likely due to the different wind field spatial resolution. However this small deviation does not alter the conclusions of this work, as will be shown later.

4 Results

Composites of wave parameters have been calculated for different cyclone characteristics in order to explore and isolate their impact on the wave fields. These features include the translational speed of the cyclone (TS), its intensity and its size. Each case is described in detail in this section.

4.1 Translational speed of cyclones

Figure 2 shows the spatial distribution of Hs (total as well as wind-sea and swell components) under cyclones for three ranges of TS: < 5 m/s, 5 to 10 m/s and > 10 m/s. These values have been chosen to ensure a representative sample in each case (note that the number of cyclones is indicated in the figure). In all cases higher waves are found in the rear-right quadrant of the cyclone, where winds are stronger because the cyclone wind velocity adds up to the cyclone displacement (the opposite occurs for left quadrants). This is in agreement with the general rule that more intense winds and larger waves develop in the rear right quadrant (Cline, 1920; Tannehill, 1936).

As the TS increases, wind speed anomalies increases together with Hs and the corresponding zones in the rear-right quadrant become more localized. Also the overall left-right asymmetry becomes more evident with higher TS. The uncertainties, plotted as dark purple lines, reach no more than 10% of Hs inside cyclones (green circle), indicating thus that the results are significant.

The spatial distribution of $H_s^{wind\text{-}sea}$ (Figure 2, middle row) mimics to a large extent that of Hs. Since $H_s^{wind\text{-}sea}$ is only related to local wind forcing, the changes with TS are more localized and well defined, with increasing left-right asymmetry as TS grows. In the center of the cyclone, $H_s^{wind\text{-}sea}$ values are negative (i.e. below average) for all TS. This is the reason for the low values found for Hs. In contrast to $H_s^{wind\text{-}sea}$, H_s^{swell} (Figure 2, bottom row) displays lower values where winds are stronger (rear-right sector) and higher at the cyclone center. H_s^{swell} increases with larger TS. For fast moving cyclones (TS >10 m/s) maxima extend towards the tail of the structure. It is worth noting that H_s^{swell} is directed towards the center of the cyclone in those areas where values are higher.

The edge of the cyclone derived from the atmospheric fields (green circles) does not always match its imprint in the pattern of Hs. Actually, the center defined by the wave field shows a downward shift, with this displacement being larger for faster cyclones. This effect is especially evident for $H_s^{wind\text{-}sea}$, which can be explained by the more smoothed downscaled wind fields as mentioned above.

4.2 Strength of cyclones

The cyclone intensity has been defined on the basis of the maximum wind speed observed. Again three ranges of maximum wind speed have been explored, namely smaller than 6 m/s, between 6 and 9 m/s and larger than 9 m/s. The resulting composites are mapped in Figure 3 for Hs and its components $H_s^{wind\text{-}sea}$ and H_s^{swell}, showing that the impact of the intensity is very strong for all wave parameters. For the weakest cyclones, maximum Hs is only 0.2 m while it reaches 1.8 m for the most intense (Figure 3, upper row). Higher H_s and $H_s^{wind\text{-}sea}$ are found in all cases at the rear-right sector, where winds are stronger. Interestingly, unlike for faster cyclones, in this case stronger cyclones follow the wind patterns more closely (see for example the center of $H_s^{wind\text{-}sea}$ without any displacement).

On the other hand, the wave age is dependent upon the cyclone intensity, since it is inversely proportional to S. Therefore, the same classification has been used to build the WA composites (Figure S2). Those areas in Figure S2 in which the uncertainty in WA is of the same order as its value have been shadowed in gray to avoid misinterpretations. The smallest values of WA are found in the rear-right sector where wind speed is higher. As expected, the WA decreases with more intense cyclones, and simultaneously the left right symmetry is enhanced. The center of the cyclone is the region where WA reaches its maximum, indicating that it corresponds to an area of swell predominance. This is in agreement with the findings in Figure 3.

4.3 Size of cyclones

Composites of Hs have been built for three different cyclone radii: smaller than 500 km, between 500 and 600 km and above 600 km. The results, displayed in Figure 4, indicate that the largest cyclones show stronger winds and therefore higher Hs (Figure 4, upper row). These fields thus allow linking the cyclone size to its intensity, a relationship that will be further explored in the next section. Values of H_s are around 0.6 m for the smallest cases and reach 1.6 m for the largest cyclones. The same applies to $H_s^{wind\text{-}sea}$ (middle row), whereas H_s^{swell} also increases at the center of the cyclone for the largest events. In fact, the largest cyclones show a wave pattern more consistent with the expected winds in terms of their spatial structure and the coincidence of their centers.

Discussion and concluding remarks

To our knowledge, this is the first time that this type of analysis has been applied in a marginal sea for extra-tropical cyclones, whose strength is within the same range that the much more studied tropical storms (15-30 m/s). Hence, our results are complementary to earlier works aimed at describing the wave climate under the influence of TCs, which are more intense perturbations that develop in large basins and with different spatial footprints on surface waves (e.g. Timmermans *et al.*, 2017).

Our findings point out that under the influence of cyclones, H_s anomalies as well as $H_s^{wind\text{-}sea}$ and H_s^{swell} anomalies, significantly increase when these events are more intense, as expected. However, these changes are far from homogeneous; as cyclone velocity adds up to local wind on the right side of the cyclone, it has a stronger impact on wind speed in this sector, and therefore it is where the highest H_s and $H_s^{wind\text{-}sea}$ are found. This effect is more intense and localized with larger TS and, in particular, there is an increase in the left-right asymmetry and a backward displacement of the center defined by waves direction from the theoretical cyclone center (Figure 2). We have found that the highest waves are located in the rear-right sector of the cyclone, where winds are stronger (Figure 2). This result contrasts with earlier assessments in which the front-right quadrant has been identified as the area of maximum wave height (Wright *et al.*, 2001; Moon *et al.*, 2004; Doyle *et al.*, 2012). However, all these cases focused on TCs. Most studies show that in the case of the hurricanes the largest waves are located in the front-right sector, being linked to the swell generated by the TC that become trapped within the cyclone due to a resonance effect occurring when the perturbation travels at a speed close to the wave propagation speed (see Moon *et al.* (2003) for a detailed explanation of this dynamic fetch). In the case of hurricanes, this swell can be even larger than the locally generated waves. Conversely, in the Western Mediterranean this resonance effect cannot be developed due to the small size of the basin with respect to the size of the cyclones: the average radius of the cyclones we are considering is 551 km whereas in our study the center of the furthest cyclone is only 238 km from the closest shoreline. On the other hand, a recent study of Hwang and Walsh (2016) using synthetic aperture radar (SAR) measurements of wave parameters under TCs identified the rear-right region as the one with more intense air-sea exchange of energy and momentum by using empirical fetch growth functions (see Figures 10 and 11 therein). Winds over 35 m/s may stop wave growth, which will occur specially in the rear-right quadrant where both wind is stronger and air-sea exchange more efficient. This wave breaking at an earlier stage will be accompanied by whitecaps on the ocean surface (Hwang and Walsh, 2016). In this study the absence of the trapping resonance effect and of hurricane force winds, suggests that, in agreement with our results, higher waves develop on the rear right side. The enhancement of the left-right asymmetry reported above is also found for cyclones with increasing radii, which are more powerful than small ones. Nevertheless, we cannot establish a robust statistical relationship between TS and R on the basis of our data set due to the limitations in the determination of TS, as will be further discussed below.

The separation of total significant wave height into its $H_s^{wind\text{-}sea}$ and H_s^{swell} components has revealed that the effects of increasing cyclone intensity are opposed. With stronger cyclones $H_s^{wind\text{-}sea}$ increases in the right-rear quadrant and decreases in the cyclone center, whereas H_s^{swell} drops down in the right-rear sector and reaches its maximum at the center, although with values up to three times smaller than the $H_s^{wind\text{-}sea}$. Wave directions of the swell component in Figures 2, 3 and 4 confirm that these waves were generated in the rear-right sector and moved towards the center. The overall picture of the combination of the two components is consistent with the WA results (Figure S2), with higher values in the cyclone center that identify the swell component. For the sake of completeness, we have also repeated the composites for the fetch (not shown) that led to the same conclusion: fetch increases along with swell propagation, from the rear-right quadrant towards the cyclone center.

This swell propagation is, again, hardly comparable with what happens with TCs because of the relative small dimensions and the topographic complexity of the Western Mediterranean Sea. $H_s^{wind\text{-}sea}$ under TCs radiates out of the maximum wind speed zone (right side of a cyclone moving upwards). For instance, in the case of hurricane Bonnie, swell was observed roughly aligned in with the cyclone track and outside the cyclone (Wright *et al.*, 2001; Holthuijsen *et al.*, 2012).

In addition to the spatial patterns of the waves generated by the cyclones, it is also interesting to investigate the relationship between the maximum Hs reached in each event, H_s^{max}, and the cyclones characteristics (TS, intensity and radii). In our data set we found that H_s^{max} is not correlated to TS, despite faster cyclones are associated with more intense events and thus with stronger winds. Yet, we conclude that this apparent contradiction is due to the way we have estimated TS, a methodology that is clearly limited by the spatial resolution (1.125° ≈ 125 km) of the cyclone data set (Campins *et al.*, 2011). For example, one cyclone during two consecutive time steps (separated 6 hours to each other) can apparently remain stationary at the same location and, at the third time step 6 hours later, suddenly jump to a neighboring grid point; in this case the estimated velocities between two consecutive time steps can differ from the real velocity because the cyclone has moved continuously.

On the other hand, according to the Figures 3 and 4, H_s^{max} is related to the cyclone radii and maximum wind intensity (the correlation coefficients R are 0.40 and 0.93, respectively). Figure 5 represents the scatter points of H_s^{max} and the maximum wind speed for each cyclone. The curve that best fits both variables, among a set of polynomials of different order, is given by:

$$H_s^{max} = 0.01S^2_{max} + 0.165S_{max} - 0.211 \qquad (1)$$

Where S_{max} represents the maximum wind speed. Adding the cyclone radius to this relationship does not improve the fitting (the correlation coefficient increases by 0.005 at the best), because the radius and the maximum winds are correlated to each other. As expected, H_s^{max} is highly dependent on the maximum wind speed because the transfer of energy from the atmosphere to the sea is higher. In addition, H_s^{max} corresponds to a large extent to wind-sea since these waves are locally dominant over swell in all our case studies.

Despite some limitations in the cyclones database such as the spatial coarse resolution or the assumption that cyclones are perfect circles, this study demonstrates a clear and spatially heterogeneous imprint of cyclones on wave patterns. This pattern, predicting the highest waves in the rear-right sector, differs from that observed in the much more investigated cases with TCs. And so do the potentially hazardous impacts of these phenomena. Thus, depending on the location and the direction of propagation of the cyclone, the area where the highest waves will be developed can be easily forecasted. Moreover, the relationship between maximum H_s and maximum wind speed permits the estimation of the size of these waves parameterized with the atmospheric characteristics of the event, which can be relevant for coastal protection. In principle, a cyclone climatology in which the intensity, size, direction and TS of each event is accurately computed, could serve to identify the coastal sectors that are more exposed to the high waves generated by the cyclones. With the present climatology for the Western Mediterranean basin though, the assessment of coastal vulnerability is hampered by the low spatial resolution and difficulty to estimate the TS with enough precision. Yet, we anticipate that a higher resolution data set could have utility for such practical purposes and would allow to focus especially on the most intense episodes.

Acknowledgments

This work was partially supported by the Research Project CLIMPACT (CGL201454246-C21-R, AEI/FEDER, UE) funded by the Spanish Ministry of Economy. T. Toomey is grateful to the Région Bretagne JALI supporting grant. J.M. Sayol is hired under the NWO-VIDI grant number 397 864.13.011. J.M. Sayol thanks Prof. Leo Oey for organizing the Princeton Journal Club, an inspiration for this work. G. Jordà acknowledges a Ramón y Cajal contract (RYC-2013-14714) funded by the Spanish Ministry of Economy and the Regional Government of the Balearic Islands

References

Besio G., R. Briganti, A. Romano, L. Mentaschi, and P. De Girolamo (2017), Time clustering of wave storms in the mediterranean sea, *Natural Hazards and Earth System Sciences*, 17(3), 505–514, doi:10.5194/nhess-17-505-2017.

Campins J., A. Genovés, M. A. Picornell, and A. Jansà (2011), Climatology of mediterranean cyclones using the era-40 dataset, *International Journal of Climatology*, 31(11), 1596–1614, doi:10.1002/joc.2183.

Cardone V. J., R. E. Jensen, D. T. Resio, V. R. Swail, and A. T. Cox (1996), Evaluation of contemporary ocean wave models in rare extreme events: The halloween storm of october 1991 and the storm of the century of march 1993, *Journal of Atmospheric and Oceanic Technology*, 13(1), 198–230, doi: 10.1175/1520-0426(1996)013<0198:EOCOWM>2.0.CO;2

Cline I. M. (1920), Relation of changes in storm tides on the coast of the gulf of mexico to the center and movement of hurricanes, *Monthly Weather Review*, 48(3), 127–146, doi:10.1175/1520-0493(1920)48<127:ROCIST>2.0.CO;2.

da Rocha R. P., S. Sugahara, and R. B. da Silveira (2004), Sea waves generated by extratropical cyclones in the south atlantic ocean: Hindcast and validation against altimeter data, *Weather and Forecasting*, 19(2), 398–410, doi:10.1175/1520-0434(2004)019<0398:SWGBEC>2.0.CO;2.

Dacre H. F., M. K. Hawcroft, M. A. Stringer, and K. I. Hodges (2012), An extratropical cyclone atlas: A tool for illustrating cyclone structure and evolution characteristics, *Bulletin of the American Meteorological Society*, 93(10), 1497–1502, doi:10.1175/BAMS-D-11- 00164.1.

Déqué, M. and J.P. Piedelievre (1995), High resolution climate simulation over Europe, *Cimate Dynamics*, 11 (1995), 321-339

Déqué, M., C. Devreton, A. Braun, D. Cariolle (1994) The Arpege/Ifs atmosphere model – a contribution to the French community climate modelling, *Climate Dynamics*, 10(4–5) (1994), 249-266

De Zolt S., P. Lionello, A. Nuhu, and A. Tomasin (2006), The disastrous storm of 4 november 1966 italy, *Natural Hazards and Earth System Sciences*, 6(5), 861–879, doi:10.5194/nhess-6-861-2006.

Doyle J., P. Black, C. Amerault, S. Chen, and S. Wang (2012), Wind-wave interaction under hurricane conditions: a decade of progress, in *Proceedings of ECMWF Workshop on Ocean Waves, 25-27 June*, edited by ECMWF.

Fan Y., I. Ginis, T. Hara, C. W. Wright, and E. J. Walsh (2009), Numerical simulations and observations of surface wave fields under an extreme tropical cyclone, *Journal of Physical Oceanography*, 39(9), 2097–2116, doi:10.1175/2009JPO4224.1.

Guimarães P. V., L. Farina, and E. E. Toldo Jr. (2014), Analysis of extreme wave events on the southern coast of Brazil, *Natural Hazards and Earth System Sciences*, 14(12), 3195– 3205, doi:10.5194/nhess-14-3195-2014.

Harley M. D., I. L. Turner, M. A. Kinsela, J. H. Middleton, P. J. Mumford, K. D. Splinter, M. S. Phillips, J. A. Simmons, D. J. Hanslow, and A. D. Short (2017), Extreme coastal erosion enhanced by anomalous extratropical storm wave direction, *Scientific Reports*, 7(1), 6033, doi:10.1038/s41598-017-05792-1.

Holthuijsen L. H., M. D. Powell, and J. D. Pietrzak (2012), Wind and waves in extreme hurricanes, *Journal of Geophysical Research: Oceans*, 117(C9), n/a–n/a, doi:10.1029/2012JC007983, c09003.

Hwang P. A., and E. J. Walsh (2016), Azimuthal and radial variation of windgenerated surface waves inside tropical cyclones, *Journal of Physical Oceanography*, 46(9), 2605–2621, doi:10.1175/JPO-D-16-0051.1.

Innocentini V., and E. D. S. C. Neto (1996), A case study of the 9 August 1988 South Atlantic storm: numerical simulations of the wave activity, *Weather and Forecasting*, 11(1), 78– 88, doi:10.1175/1520-0434(1996)011<0078:ACSOTA>2.0.CO;2.

Jansà A. (1997), A general view about mediterranean meteorology: cyclones and hazardous weather, *INM/WMO International Symposium on cyclones and hazardous weather in the Mediterranean, Palma de Mallorca.*

Jordà G., D. Gomis, E. Alvarez Fanjul, and S. Somot (2012), Atmospheric contribution to Mediterranean and nearby Atlantic sea level variability under different climate change scenarios, *Global and Planetary Change*, 80-81, 198–214, doi:https://doi.org/10.1016/j.gloplacha.2011.10.013.

Lionello P., P. Malanotte-Rizzoli, and R. Boscolo (2006), *Mediterranean Climate Variability*, 438 pp., Elsevier.

Lionello P., I. F. Trigo, V. Gil, M. L. R. Liberato, K. M. Nissen, J. G. Pinto, C. C. Raible, M. Reale, A. Tanzarella, R. M. Trigo, S. Ulbrich, and U. Ulbrich (2016), Objective climatology of cyclones in the Mediterranean region: a consensus view among methods with different system identification and tracking criteria, *Tellus A: Dynamic Meteorology and Oceanography*, 68(1), 29,391, doi:10.3402/tellusa.v68.29391.

Maheras P., H. Flocas, I. Patrikas, and C. Anagnostopoulou (2001), A 40-year objective climatology of surface cyclones in the Mediterranean region: spatial and temporal distribution, *International Journal of Climatology*, 21(1), 109–130, doi:10.1002/joc.599.

Martínez-Asensio A., M. Marcos, G. Jordà, and D. Gomis (2013), Calibration of a new wind-wave hindcast in the Western Mediterranean, *Journal of Marine Systems*, 121-122 (Supplement C), 1 – 10, doi:https://doi.org/10.1016/j.jmarsys.2013.04.006.

Moon I.-J., I. Ginis, T. Hara, H. L. Tolman, C. W. Wright, and E. J. Walsh (2003), Numerical simulation of sea surface directional wave spectra under hurricane wind forcing, *Journal of Physical Oceanography,* 33(8), 1680–1706, doi:10.1175/2410.1.

Moon I.-J., I. Ginis, and T. Hara (2004), Effect of surface waves on airsea momentum exchange. part II: Behavior of drag coefficient under tropical cyclones, *Journal of the Atmospheric Sciences*, 61(19), 2334–2348, doi:10.1175/1520-0469(2004)061<2334:EOSWOA>2.0.CO;2

Nissen K. M., G. C. Leckebusch, J. G. Pinto, D. Renggli, S. Ulbrich, and U. Ulbrich (2010), Cyclones causing wind storms in the mediterranean: characteristics, trends and links to large- scale patterns, *Natural Hazards and Earth System Sciences*, 10(7), 1379– 1391, doi:10.5194/nhess-10-1379-2010.

Picornell M., A. Jans`a, A. Genov´es, and J. Campins (2001), Automated database of mesocyclones from the HIRLAM(INM)-0.5° analyses in the western Mediterranean, *International Journal of Climatology*, 21(3), 335–354, doi:10.1002/joc.621.

Rudeva, I., and S.K. Gulev (2007) Climatology of cyclone size characteristics and their changes during the cyclone life cycle, *Monthly Weather Review*, 135, 2568- 2587, doi: 10.1175/MWR3420.1

Sartini L., F. Cassola, and G. Besio (2015), Extreme waves seasonality analysis: an application in the Mediterranean Sea, *Journal of Geophysical Research: Oceans*, 120 (9), 6266– 6288, doi:10.1002/2015JC011061.

Stephens S. A., and D. Ramsay (2014), Extreme cyclone wave climate in the Southwest Pacific Ocean: Influence of the El Niño Southern Oscillation and projected climate change, *Global and Planetary Change*, 123(Part A), 13 – 26, doi:https://doi.org/10.1016/j.gloplacha.2014.10.002.

Tannehill I. R. (1936), Sea swells in relation to movement and intensity of tropical storms, *Monthly Weather Review*, 64(7), 231–238, doi:10.1175/1520-0493(1936)64<231b:SSIRTM>2.0.CO;2.

The Wamdi Group (1988), The WAM Model-A Third Generation Ocean Wave Prediction Model, *Journal of Physical Oceanography*, 18(12), 1775–1810, doi:10.1175/1520-0485(1988)018<1775:TWMTGO>2.0.CO;2.

Timmermans B., D. Stone, M. Wehner, and H. Krishnan (2017), Impact of tropical cyclones on modeled extreme wind-wave climate, *Geophysical Research Letters*, 44(3), 1393–1401, doi:10.1002/2016GL071681, 2016GL071681.

Trigo I. F., T. D. Davies, and G. R. Bigg (1999), Objective climatology of cyclones in the mediterranean region, Journal of Climate, 12(6), 1685–1696, doi:10.1175/1520-0493(2002)130<0549:COCMIT>2.0.CO;2.

Trigo I. F., G. R. Bigg, and T. D. Davies (2002), Climatology of Cyclogenesis Mechanisms in the Mediterranean, *Monthly Weather Review,* 130(3), 549–569, doi:10.1175/1520-0493(2002)130<0549:COCMIT>2.0.CO;2.

Wright C. W., E. J. Walsh, D. Vandemark, W. B. Krabill, A. W. Garcia, S. H. Houston, M. D. Powell, P. G. Black, and F. D. Marks (2001), Hurricane directional wave spectrum spatial variation in the open ocean, *Journal of Physical Oceanography*, 31(8), 2472–2488, doi:10.1175/1520-0485(2001)031<2472:HDWSSV>2.0.CO;2..

426

Figure captions

Figure 1. Spatial distribution of Hs over the Western Mediterranean for the same cyclone at four different time steps. Black arrows represent the wind field and the cyclone is plotted as a green circle.

Figure 2. Spatial distribution of H_s, $H_s^{wind\text{-}sea}$, and H_s^{swell} for a TS of 5 m/s or less (left), between 5 and 10 m/s (center) and 10 m/s or more (right). Black arrows represent waves mean direction, dark purple contours represent the ME (order of 10^{-1} m here) while white contours show zones of maximum wind speed anomalies. N indicates the number of observations used.

Figure 3. Spatial distribution of H_s, $H_s^{wind\text{-}sea}$, and H_s^{swell} for a maximum wind speed (S_{max}) of 6 m/s or less (left), between 6 and 9 m/s (center) and 9 m/s or more (right). Black arrows represent waves mean direction, dark purple contours represent the ME (order of 10^{-1} m here) while white contours show zones of maximum wind speed anomalies. N indicates the number of observations used.

Figure 4. Comparison of total H_s, $H_s^{wind\text{-}sea}$, and H_s^{swell} for cyclones with radius of 0-500 km (left), 500-600 km (center), or 600 km and more (right). Black arrows represent waves mean direction, dark purple contours represent the ME (order of 10^{-1} m here) while white contours show zones of maximum wind speed anomalies. N indicates the number of observations used.

Figure 5. Scatter plot of H_s^{max} as a function of the maximum wind speed (S_{max}). The solid line represent the equation modeling the relation between H_s^{max} and the maximum wind speed. Dashed lines represent H_s^{max} at 99.5% prediction interval. Computed from a sample of 5178 observations (df+3), the determination coefficient is 0.863 (R^2).

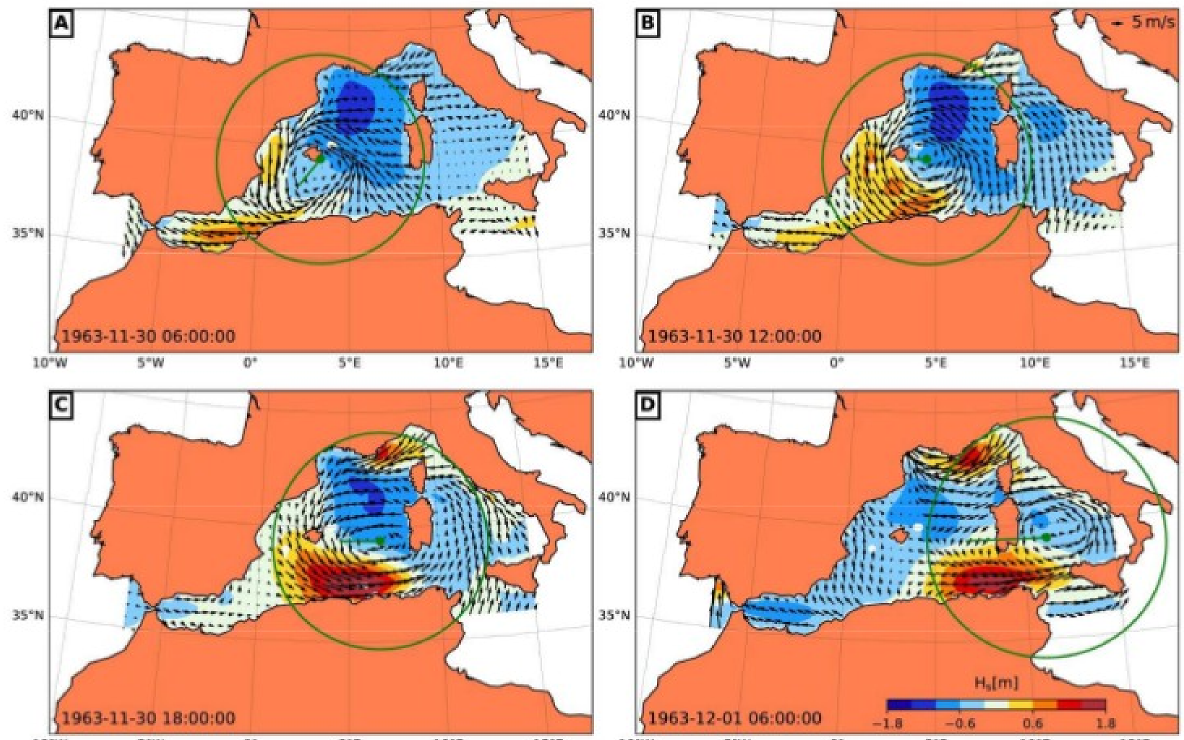

Figure 1: Spatial distribution of H_s over the Western Mediterranean for the same cyclone at four different time steps. Black arrows represent the wind field and the cyclone is plotted as a green circle.

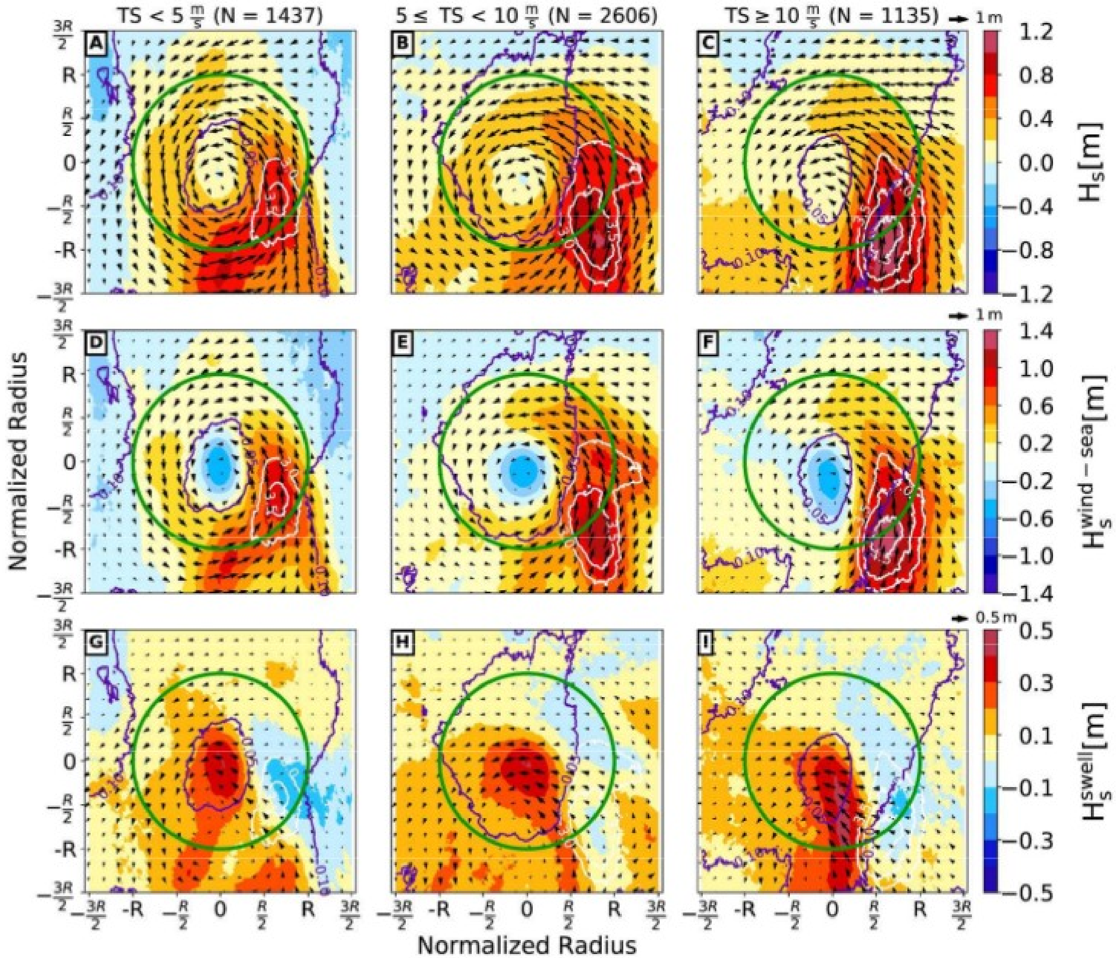

Figure 2: Spatial distribution of H_s, $H_s^{wind\text{-}sea}$, and H_s^{swell} for a TS of 5 m/s or less (left), between 5 and 10 m/s (center) and 10 m/s or more (right). Black arrows represent waves mean direction, dark purple contours represent the ME (order of 10^{-1} m here) while white contours show zones of maximum wind speed anomalies. N indicates the number of observations used.

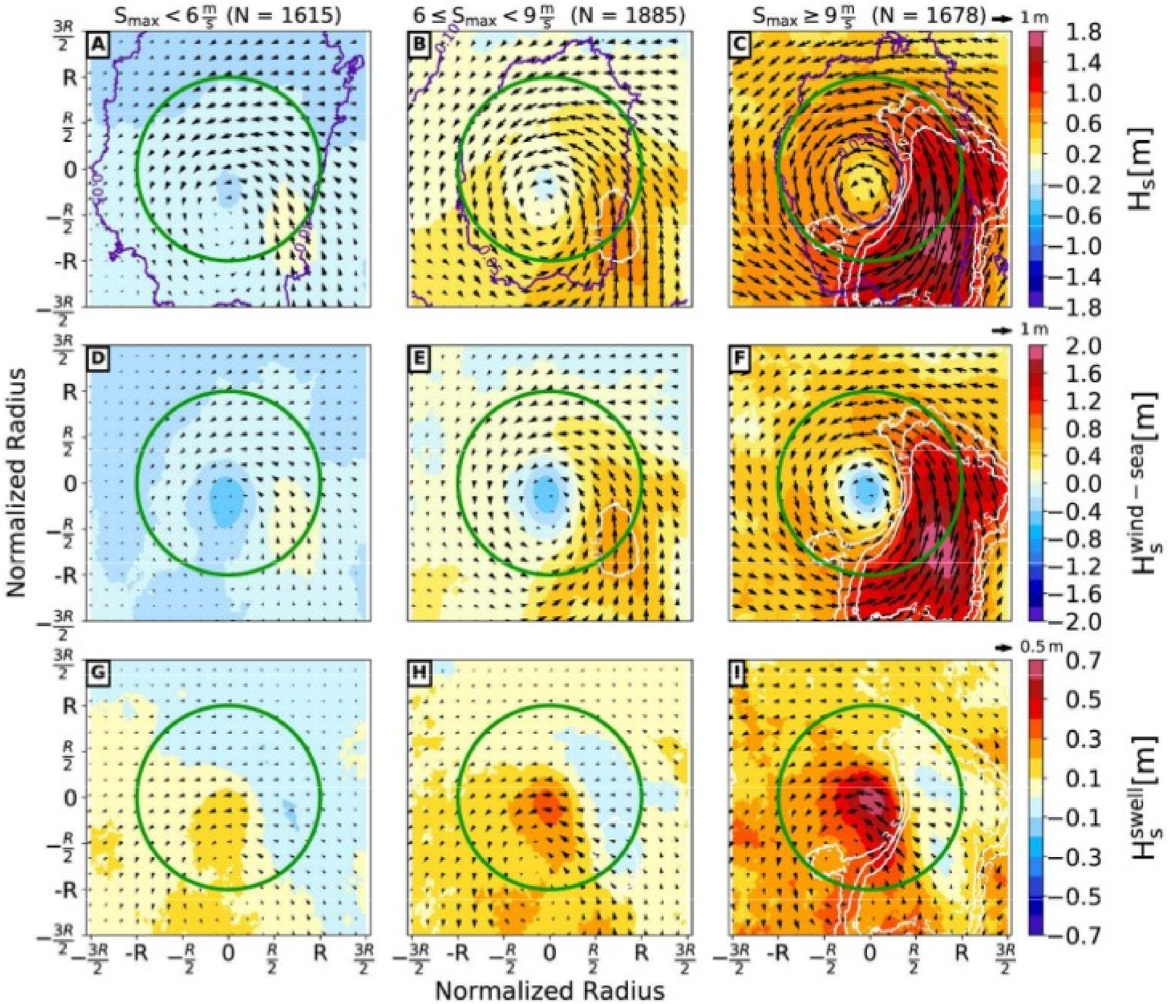

Figure 3: Spatial distribution of H_s, $H_s^{wind\text{-}sea}$, and H_s^{swell} for a maximum wind speed (S_{max}) of 6 m/s or less (left), between 6 and 9 m/s (center) and 9 m/s or more (right). Black arrows represent waves mean direction, dark purple contours represent the ME (order of 10^{-1} m here) while white contours show zones of maximum wind speed anomalies. N indicates the number of observations used.

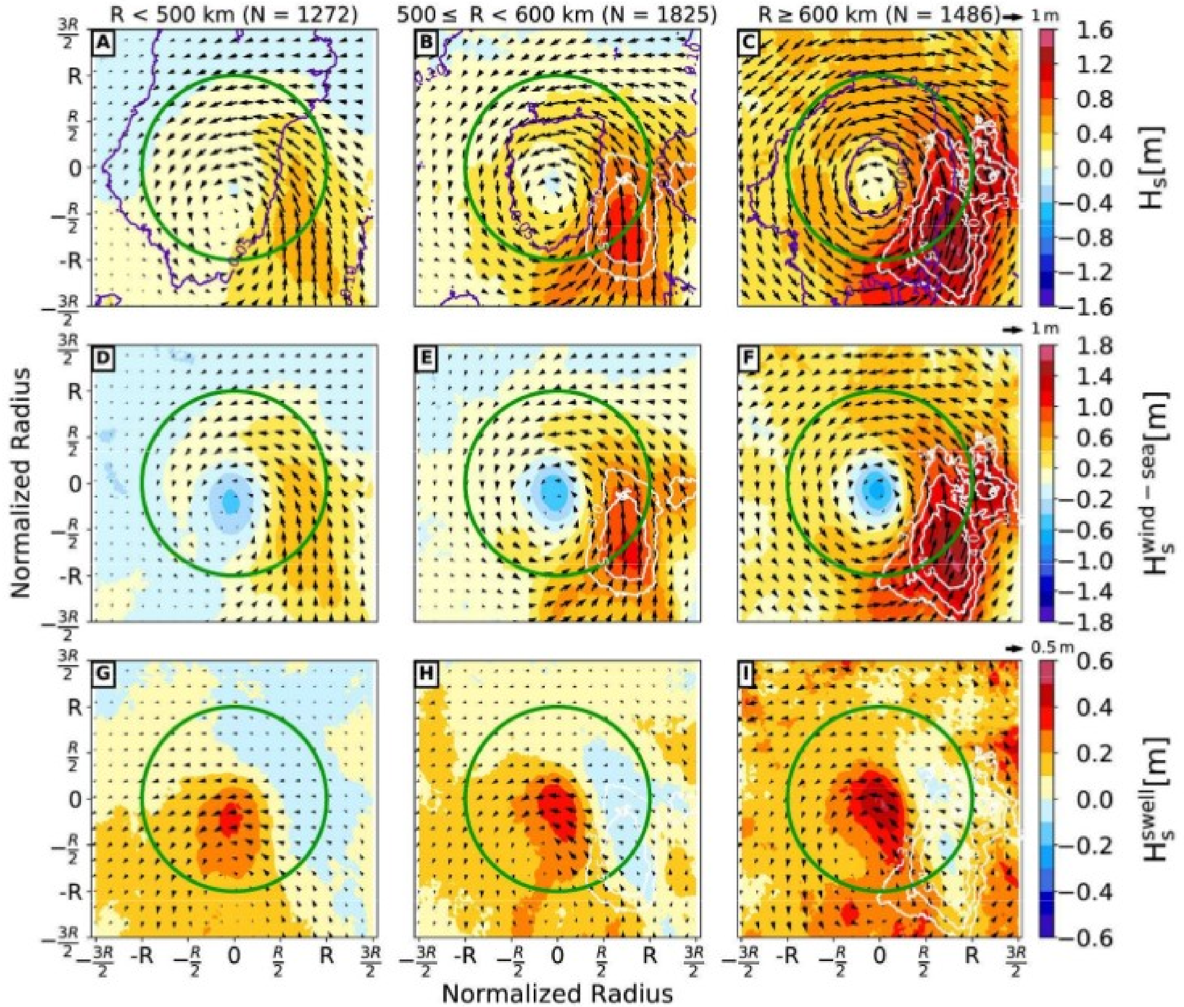

Figure 4: Comparison of total H_s, $H_s^{wind\text{-}sea}$, and H_s^{swell} for cyclones with radius of 0-500 km (left), 500-600 km (center), or 600 km and more (right). Black arrows represent waves mean direction, dark purple contours represent the ME (order of 10^{-1} m here) while white contours show zones of maximum wind speed anomalies. N indicates the number of observations used.

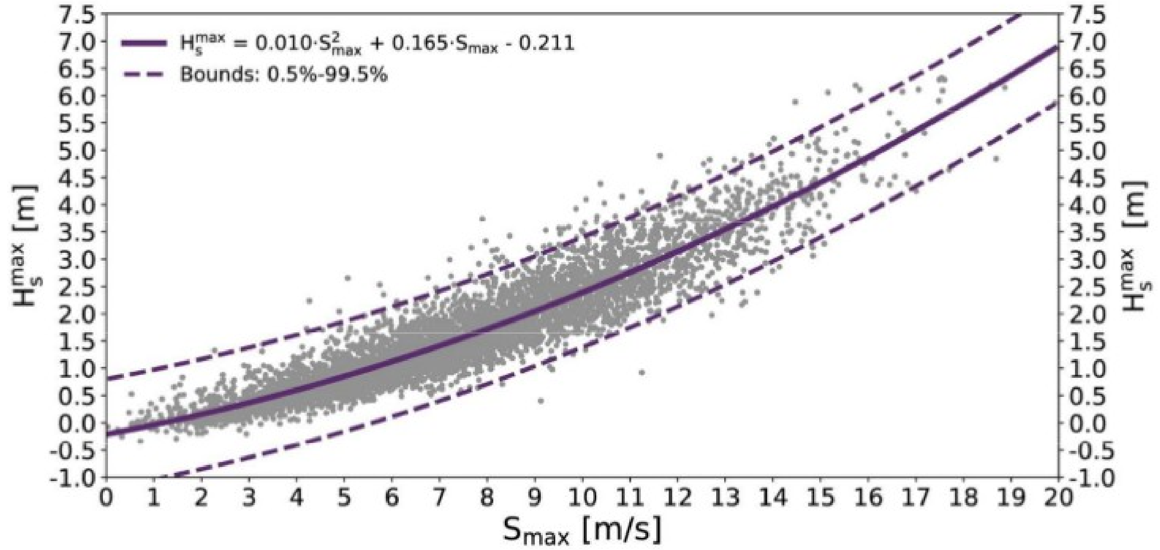

Figure 5: Scatter plot of H_s^{max} as a function of the maximum wind speed (S_{max}). The solid line represent the equation modeling the relation between H_s^{max} and maximum wind speed. Dashed lines represent H_s^{max} at 99.5% prediction interval. Computed from a sample of 5178 observations (df+3), the determination coefficient is 0.863 (R^2).